# Strength determination for band-loaded thin cylinders

Cornelia Doerich
Margi Vilnay
J. Michael Rotter

Doerich, C. Vilnay, M. and Rotter, J. M. 2018. Strength determination for band-loaded thin cylinders. *Advances in Structural Engineering*. DOI: https://doi.org/10.1177/1369433218787715

# Strength determination for band-loaded thin cylinders

Cornelia Doerich, Margi Vilnay, J. Michael Rotter

Equation Chapter 1 Section 1

## Synopsis

Cylindrical shells are often subjected to local inward loads normal to the shell that arise over restricted zones. A simple axisymmetric example is that of the ring-loaded cylinder, in which an inward line load around the circumference causes either plasticity or buckling. The ring-loaded cylinder problem is highly relevant to shell junctions in silos, tanks and similar assemblies of shell segments. The band load is similar to the ring load in that a band of inward axisymmetric pressure is applied over a finite height: when the height is very small, the situation approaches the ring loaded case: when the height is very large, it approaches the uniformly pressurised case. This paper first thoroughly explores the two limiting cases of plastic collapse and linear bifurcation buckling, which must both be fully defined before a complete description of the non-linear and imperfection sensitive strengths of such shells can be described within the framework of the European standard for shells EN 1993-1-6 (2007). Finally, the application of the Reference Resistance Design (RRD) over the complete range of geometries for the perfect structure is shown using the outcome of the limiting cases. (EN1993-1-6, 2007; Rotter, 2016a; 2016b; Sadowski et al., 2017).

# 1 Introduction

Cylindrical shells are often subjected to local inward loads normal to the shell that arise over restricted zones. A simple axisymmetric example is that of the ring-loaded cylinder, in which an inward line load around the circumference causes either plasticity or buckling. The ring-loaded cylinder problem is highly relevant to shell junctions in silos, tanks and similar assemblies of shell segments (Teng and Rotter, 1991a; Teng and Rotter, 1992; Teng, 2004; Teng and Rotter, 1991b; Teng and Rotter, 1991c). The band load is similar to the ring load in that a band of inward axisymmetric pressure is applied over a finite height: when the height is very small, the situation approaches the ring loaded case: when the height is very large, this approaches the uniformly

pressurised case (Batdorf, 1947; Greiner, 2004)

In the past, problems of shell buckling of this kind were often explored using finite element software and the outcomes of nonlinear elastic-plastic buckling analyses were represented using empirical fits to the results. This led to a situation in which every problem was represented by a new set of empirical fits, with no relationship between them, and no close relationship to classical or algebraic solutions that could be obtained for special cases. The conceptual framework of the European standard on shells (EN1993-1-6, 2007; Rotter and Schmidt, 2014; Rotter, 2002; Rotter, 2007) changes this situation, and requires that every problem should have two reference strengths determined as an anchoring basis: the critical buckling resistance and the plastic reference resistance. These two values are determined respectively using a Linear Bifurcation Analysis (LBA) and a Materially Nonlinear Analysis (MNA) using an ideal elastic-plastic material model.

This paper presents the outcome of these two analyses for band-loaded cylinders with a large range of radius-to-thickness ratios ($100 \leq r/t \leq 2000$), bands of pressure over a range of heights ($0.1 < h/r < 0.5$) and a relatively long cylinder (height to radius ratio $H/r > 4$). The two limiting cases of elastic buckling and plastic collapse must both be fully defined before a complete description of the non-linear and imperfection sensitive strengths of such shells can be described within the framework of the European standard for shells EN 1993-1-6 (2007). Finally, the application of the Reference Resistance Design (RRD) over the complete range of geometries for the perfect structure is shown using the outcome of the limiting cases.

## 2 Analysis and representation

The isotropic cylinders in this study were treated as made of ideal elastic-plastic material satisfying the von Mises yield criterion with normal plastic flow. All shells were analysed using the commercial software Abaqus (ABAQUS, 2017). The analyses throughout this study were conducted using S4R elements (Figure 1). In addition, the plastic collapse analysis (MNA) was conducted using an axisymmetric model (SAX1) and the full 3D model verified against its predictions. The mesh convergence was verified for appropriate sample geometries.

Each cylindrical shell was subjected to an axisymmetric band of external uniform pressure covering a height $h$ (Figure 1). The geometry was characterised by its radius to thickness ratio $r/t$,

with a range from 100 to 2000. The shell height $H$ was chosen to give a long enough cylinder so that the two reference loads were unaffected by the proximity of the boundaries. For these studies, this height was chosen principally as $H/r$=4. The thickness $t$ was used as the reference dimension so that all thicknesses, radii and heights could be treated in a single calculation. The cylinder was simply supported at the base and constrained against out-of-round deformations at the top, but free to move axially (BC2f). The material parameters were $E$=200 000 MPa, $\nu$=0.3 and $\sigma_y$=250 MPa to model mild steel. Strain hardening was excluded.

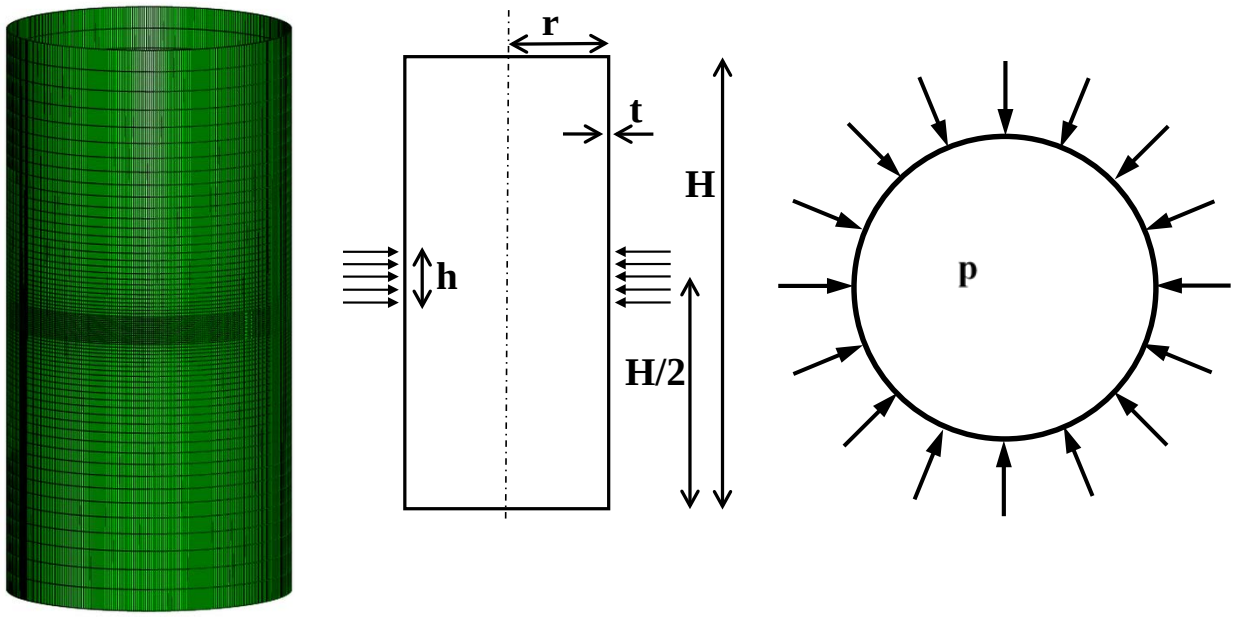


**Figure 1: Cylinder subject to axisymmetric pressure band of pressure *p* over the height *h***

## 3 The critical buckling resistance ($R_{cr}$)

Since the shells in this study are subject to external pressure, leading to circumferential compression that induces buckling, the natural reference against which the findings might be compared is that of buckling under uniform external pressure.

The original work of Batdorf (1947) and Ebner (1952) on cylinders of medium length with simply supported ends led to the linear bifurcation prediction (Greiner, 2004)

$$p_{cr} = \frac{0.855CE}{(1-\nu^2)^{0.75}}\left(\frac{r}{H}\right)\left(\frac{t}{r}\right)^{2.5} \tag{1}$$

in which the coefficient $C$ varies according to the boundary conditions (EN1993-1-6, 2007). It takes the value $C = 1.0$ for the pinned boundary conditions used here. It may be expected that the elastic critical resistance of the band loaded cylinder should relate well to this expression.

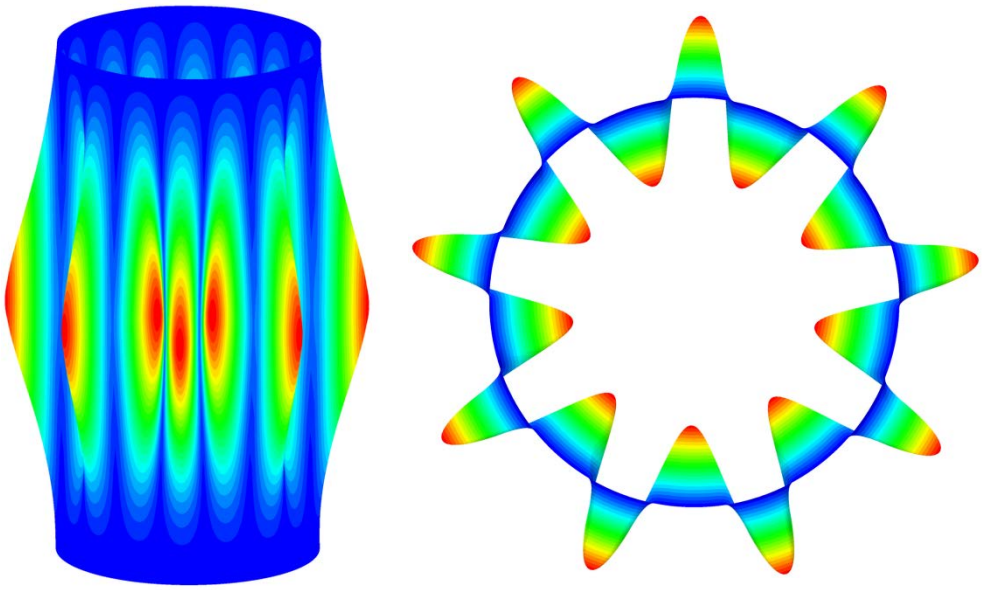

a) b)

**Figure 2: Calculated linear bifurcation mode for *r/t* = 750, *H/r* = 4 and *h/r* = 0.2**

The first study of the band loaded cylinder explored the elastic critical resistance using a Linear Bifurcation Analysis. The numerical analysis was performed on a 360° model (Figure 1). The resulting buckling modes for all geometries were similar with long waves around the circumference of the cylinder (Figure 2). Even for very small band heights, the buckles often extend over the full height of the cylinder (Figure 2 and Figure 4). The number of circumferential buckling waves decreases with increasing height of the band load towards the number of buckling waves found in the uniformly pressurised cylinder (Figure 3). This behaviour corresponds well to the behaviour of cylinders under uniform external pressure (Brush and Almroth, 1975; Greiner, 2004), where the critical number of buckling waves decreases with increased cylinder height.

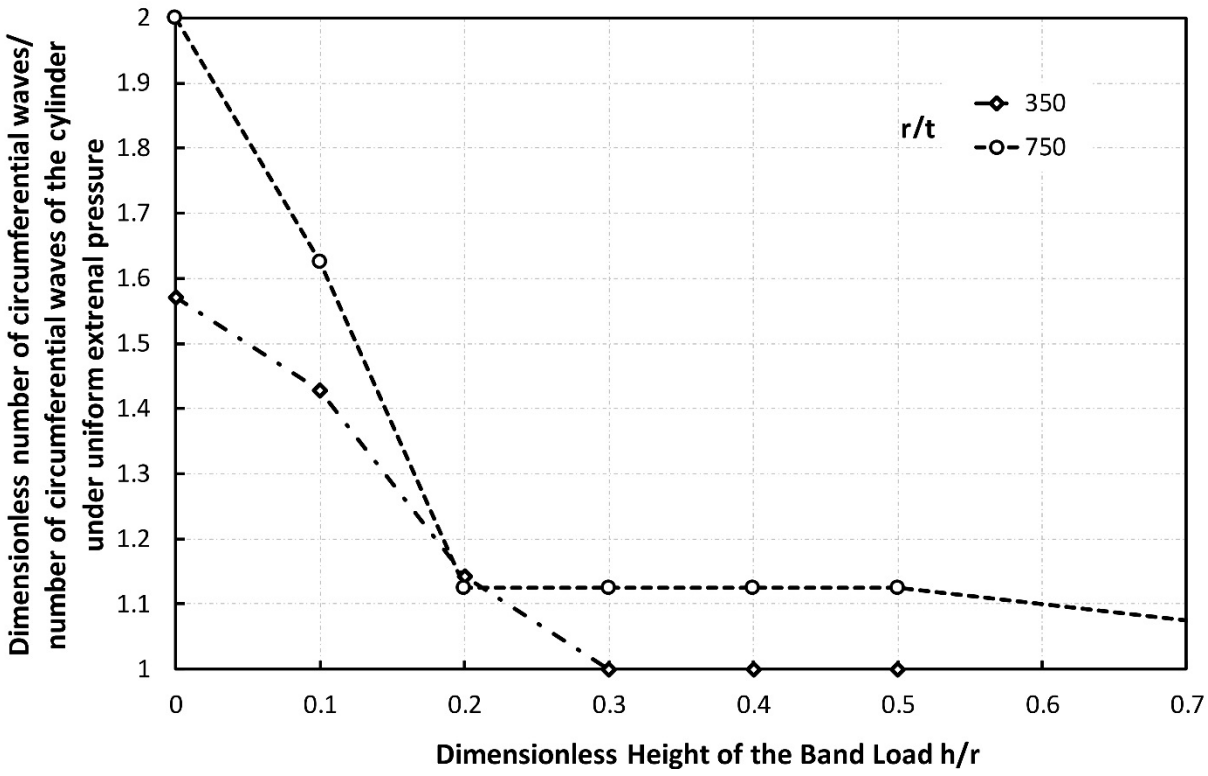


**Figure 3: Dimensionless number of circumferential buckling waves (1st eigenvalue)**

The height of this buckling mode suggests that the buckling resistance should depend strongly on the cylinder height. An expression comparable with Eq.1 may therefore be expected to be appropriate.

A selected set of calculated linear bifurcation resistances for the aspect ratio $H/r = 4$ is shown in Figure 5, where there is a clear linear variation with the inverse of the dimensionless height $h$ of the loaded band. As the loaded band height increases, the circumferential membrane stress spreads further up and down the cylinder, and with the centre of the band situated in the middle of the buckle, the bifurcation pressure naturally steadily decreases. There is a slight variation from this linear relationship at low $r/h$, where the band covers a large part of the cylinder. However, this condition leads to higher pressures than a simple linear description would give, so an approximation of the relationship as linear is satisfactory for design purposes. Ignoring these low values of $r/h$, the linear relationship is accurately described by Eq. 2.

$$p_{cr}\left(r/h\right) = E\left(C_1 \frac{r}{h} + C_2\right) \tag{2}$$

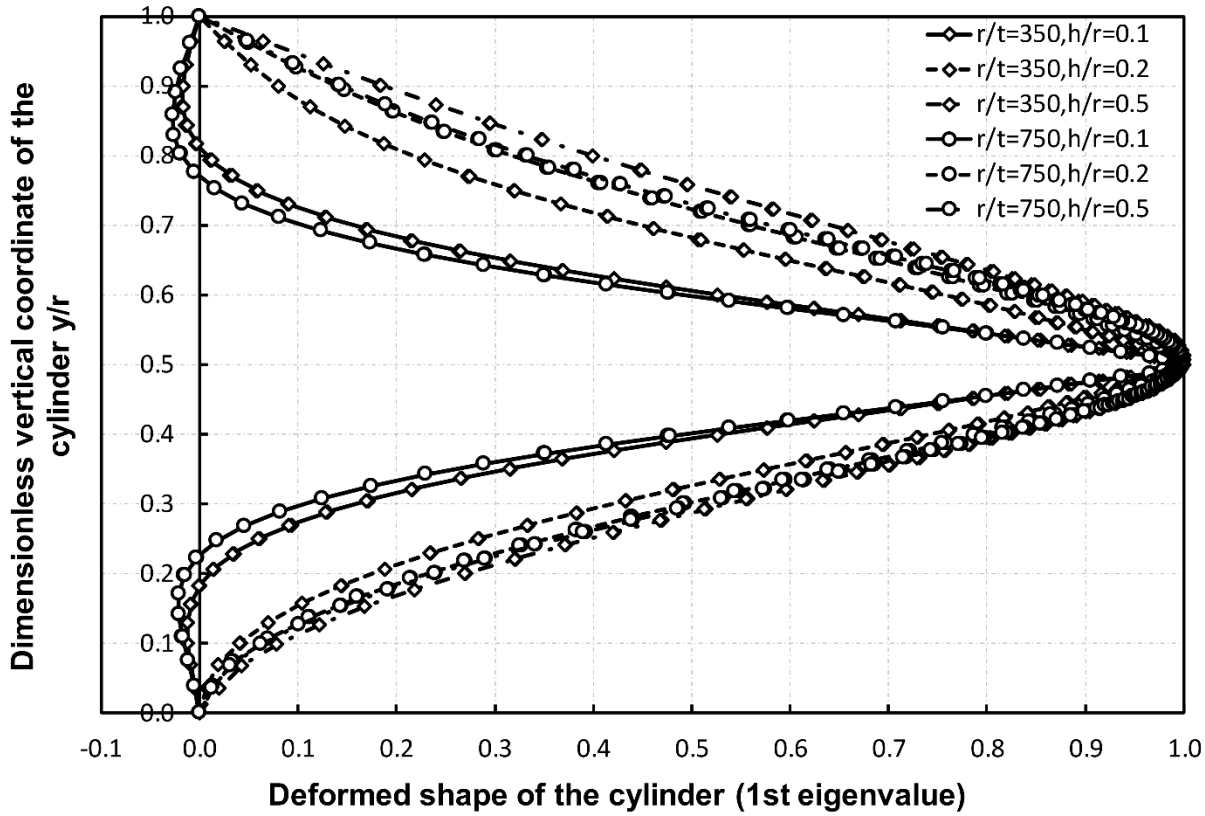


**Figure 4: Deformed shape of the cylinder (1st eigenvalue) over the height of the cylinder**

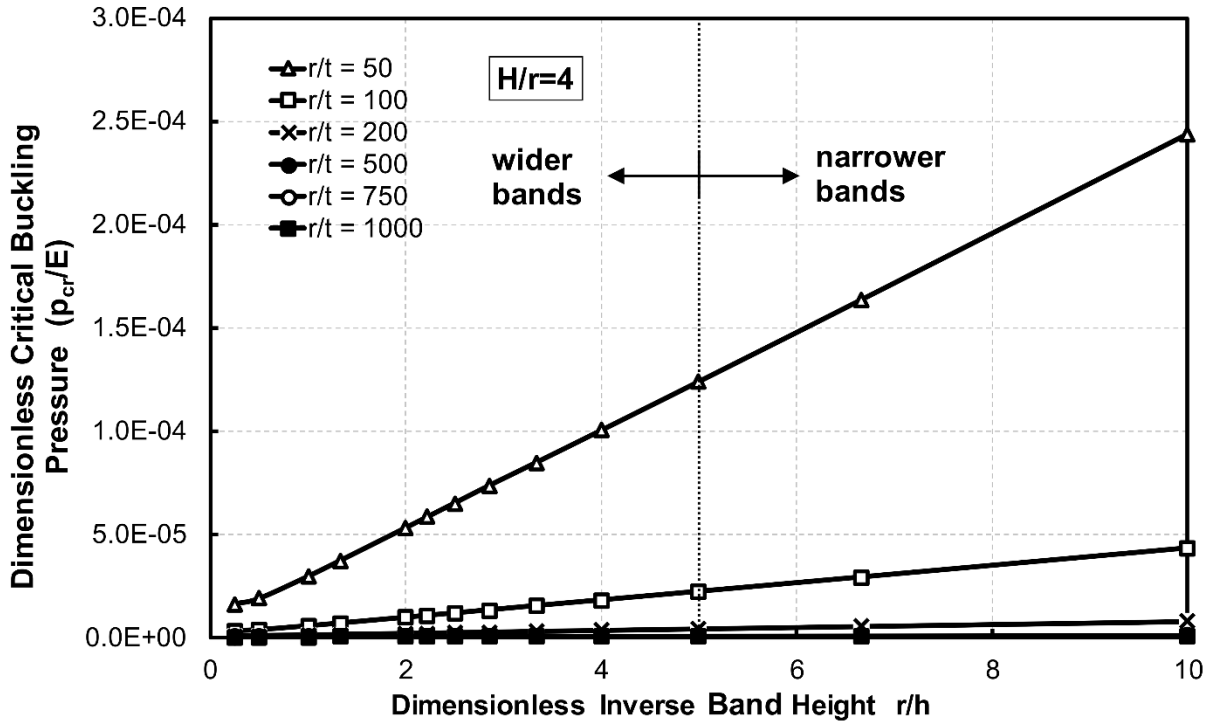


**Figure 5: Variation of the bifurcation pressure with the dimensionless inverse height of the band *h/r***

The variation of the bifurcation resistance with the radius to thickness ratio *r/t* is shown in Figure 6, where the log-log plot demonstrates a close relationship to the power law of Batdorf (1947). The exponent is close to -2.5 for all band heights. The best fit value for all calculations was found to be -2.483 with a small range from -2.481 to -2.486. It seems likely that a more precise value of the exponent in Eq. 1 would be -2.48 when the analysis is based on a more accurate shell theory (Yamaki, 1984).

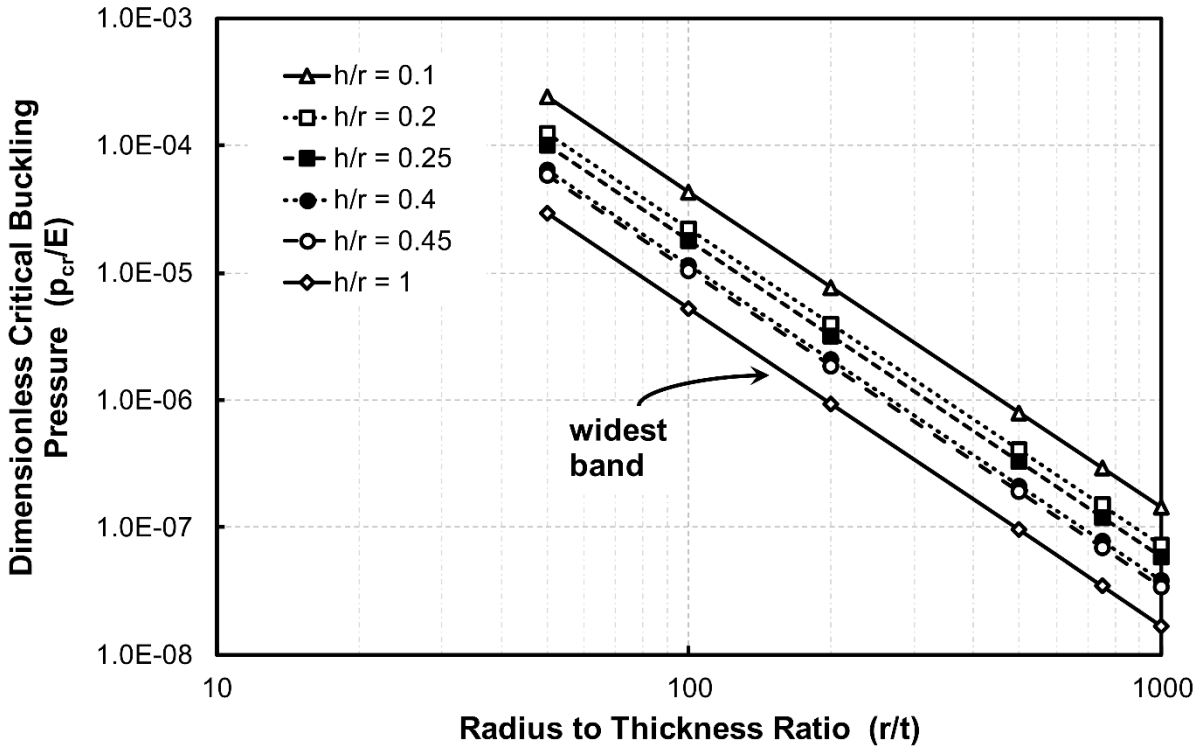


**Figure 6: Variation of the bifurcation pressure with the radius to thickness ratio r/t**

The variation of the bifurcation pressure (Figure 7) with Poisson's ratio follows the same pattern as shown in Eq. (1) (Greiner, 2004).

Combining the above findings leads to the following expression for the bifurcation pressure.

$$p_{cr}\left(r/h, t/r\right) = \frac{E}{\left(1-\nu^2\right)^{0.75}}\left\{C_3\frac{r}{h}+C_4\right\}\left(\frac{t}{r}\right)^{2.48} \tag{3}$$

in which $C_3$ = 0.364 and $C_4$ = 0.080 when $H/r$ = 4. Equation 3 produces a very good fit to the numerical results with a maximum deviation of ±5%.

It may also deduced that the buckling resistance of the cylinder under a ring line load $F_{cr}$ per unit circumference is given by

$$F_{cr} = \frac{E}{\left(1-\nu^2\right)^{0.75}}\left(C_3 r\right)\left(\frac{t}{r}\right)^{2.48} \tag{4}$$

which closely matches the numerical results for a ring loaded cylinder.

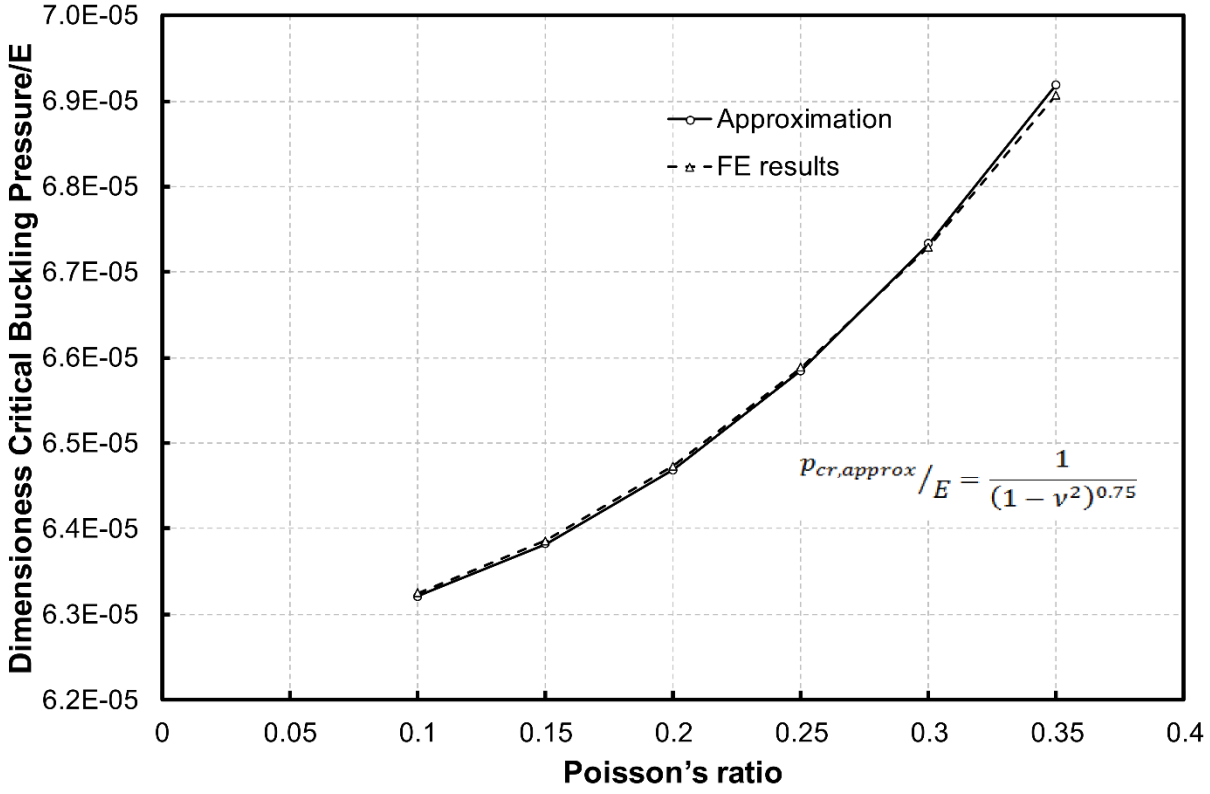


**Figure 7: Variation of the dimensionless critical buckling pressure with Poisson's ratio (r/t=350, H/r=4, h/r=0.3)**

The overall fit for *H/r = 4* is shown in Figure 8 using the dimensionless pressure with $p_{cr}$ from Eq. 3

$$p^* = \frac{p_{cr}\left(1-\nu^2\right)^{0.75}}{E}\left(\frac{r}{t}\right)^{2.48} \tag{5}$$

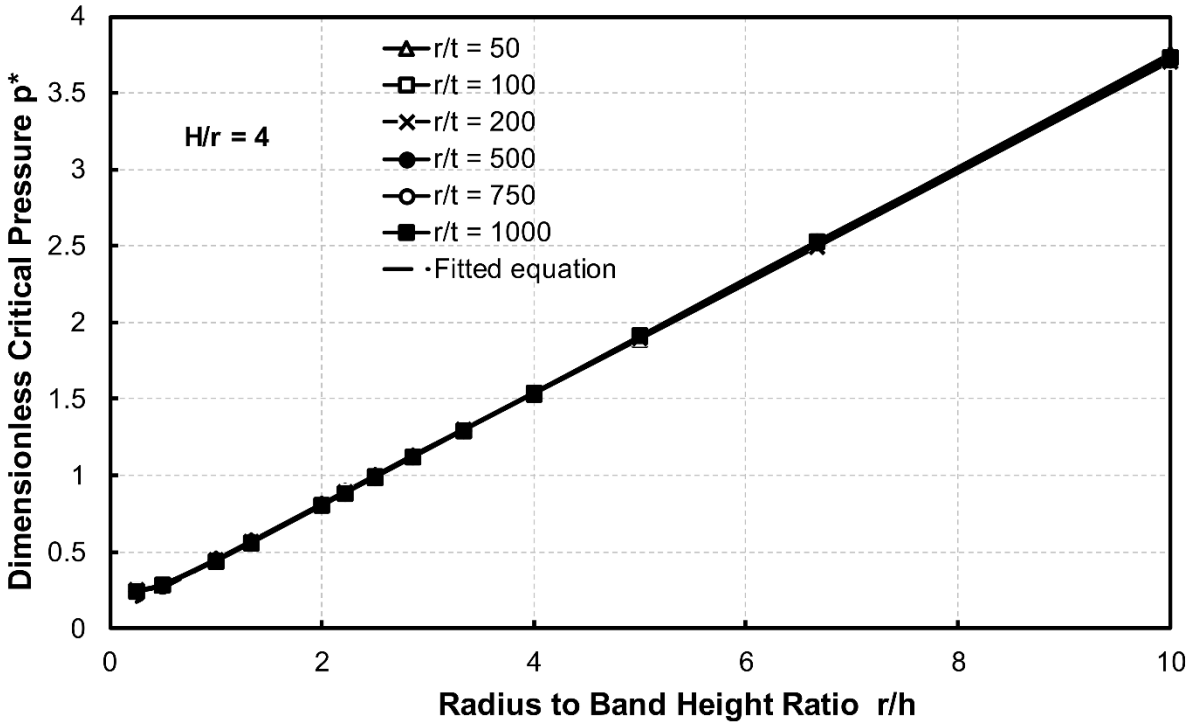


**Figure 8: Complete dimensionless description of linear bifurcation pressures for *H/r* = 4**

When different heights of cylinder were studied, it was expected that an approximately linear relationship between bifurcation pressure $p_{cr}$ and cylinder height $H$ might be found, following Eq. 1 and noting the buckling mode. However, this was found not to be the case for all common cylinder aspect ratios. This is shown in Figure 9, where the dimensionless pressure $p^*$ for all aspect ratios greater than $H/r = 2$ (which is a cylinder where the height and diameter are equal) is only very mildly dependent on the cylinder aspect ratio $H/r$.

This effect is shown more clearly in Figure 10, where the increase in bifurcation resistance from the aspect ratio $H/r = 10$ to the aspect ratios $H/r = 4$ and 2 are shown. The difference is clearly very small when the band height is low, but rises slightly for larger band heights. The difference between $H/r = 4$ and $H/r = 10$ is less than 4% for band heights $h$ less than half the cylinder radius. This shows that the expectation that the band loaded cylinder, with its buckling mode commonly extending over the full height (Figure 2) does not depend on the cylinder height $H$ as suggested by Eq. 1.

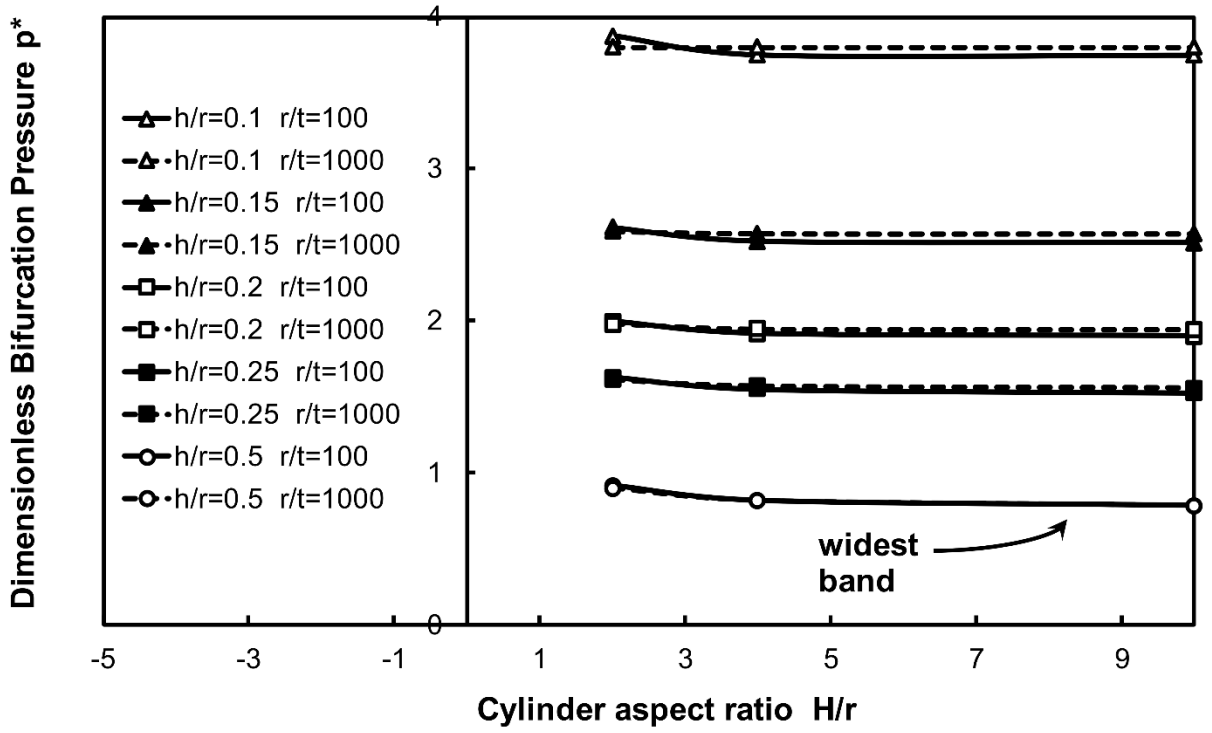


**Figure 9: Variation of dimensionless pressure with cylinder aspect ratio *H/r***

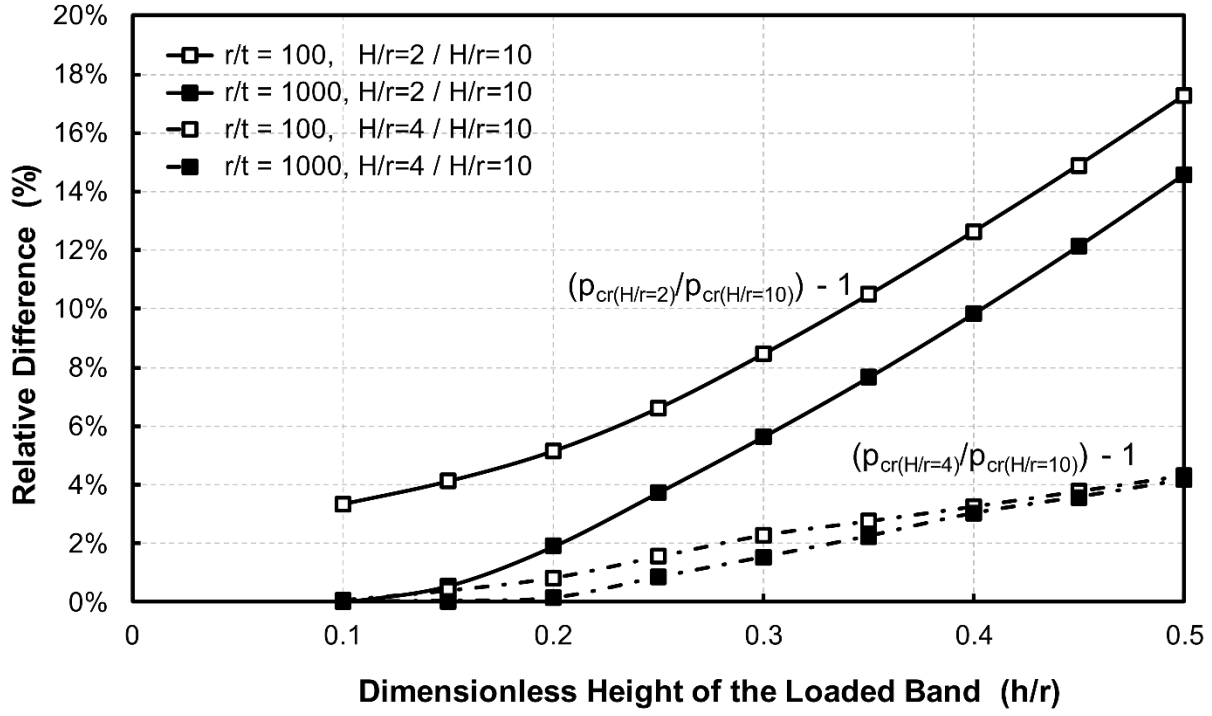


**Figure 10: Deviation of bifurcation pressure from the values for *H/r* = 10**

The empirical Eq. 3 provides a good representation of the bifurcation pressure for a band loaded cylinder, and the relatively small errors (Figure 8) indicate that this equation provides a

conservative and reasonably accurate value for design purposes.

Comparing Eqs (1) and (3), the critical difference between a uniformly externally pressurised cylinder and one carrying only a band of pressure is that whilst in the uniformly loaded case the bifurcation pressure is inversely proportional to the height of the full cylinder $H$, when it is loaded on a band this inverse proportionality is with the height of the band $h$. This finding indicates that the total applied external load dominates external pressure buckling, even when the same mode is invoked. The two bifurcation pressures vary identically with the radius to thickness ratio.

It should be noted, however, that Eq. 5 only applies to perhaps $h/r < 0.5$. The lower limit of radius to thickness ratio $r/t$ for which this result is applicable, is evidently governed by yielding, so no limitation is needed on $r/t$.

# 4 The plastic reference resistance ($R_{pl}$)

The second reference load required for Reference Resistance Design (Rotter, 2016a; 2016b) is the plastic limit resistance $R_{pl}$. This reference load is obtained from a materially nonlinear analysis MNA using small deflection theory which reaches a well defined value when a fully plastic mechanism is formed. Since the formation of this mechanism is progressive, and is only fully developed at very large displacements, the load is not easily determined accurately from a numerical analysis. Particular care is taken here to obtain precise values.

The collapse mechanism (Save and Massonnet, 1972) couples stretching and bending plastic deformations in different proportions at different points in the shell with the maximum deflection at the mid-height of the cylinder (Figure 11 and $x$=0 in Figure 12). It is notable that the band does not produce a zone of relatively uniform deflection at its centre (Figure 12), but always shows a strong peak there with a full plastic hinge. However, at full plasticity the circumferential membrane stress is remarkably uniform over this zone of significantly varying deflection (Figure 13). To accommodate the local radial displacement, the cylinder must deform in bending in the axial direction quite dramatically causing high axial bending plastic strains. However, high bending moments $m_{pl,Mises}$ (Figure 14 and Eq. 6) only develop at the two edges of the band despite the severe bending strains at the centre because the demand for a high membrane circumferential

strain at the central plastic hinge dominates the plastic strain vector (Figure 15). The plastic strain field near the load is dominated by yielding due to stretching (Figure 15), whilst that the edge of the band is dominated by yielding due to bending (Figure 15). There is, of course, a reaction circumferential bending moment $m_\theta$ (Eq. 6) (Save and Massonnet, 1972) throughout the mechanism because the strains must be axisymmetric. The bending moments at the edges of the band exceed the simple full plastic moment of the section (Figure 14) because the von Mises yield envelope (Figure 15) reaches larger moments due to the reaction circumferential bending moment ($m_{p\theta} = 0.5m_{px}$) which pushes the yield surface out to the maximum of the material von Mises ellipse. The plot of the plastic stress states throughout the yielded zone (Figure 15) reveals much interesting detail that is more widely relevant to shells under other loading conditions when a fully plastic mechanism forms.

$$m_{p\theta,Mises} = 0.5m_{px,Mises} \text{ and } m_{px,Mises} = \left(2/\sqrt{3}\right)m_{pl} \quad with \quad m_{pl} = t^2\,\sigma_y/4 \tag{6}$$

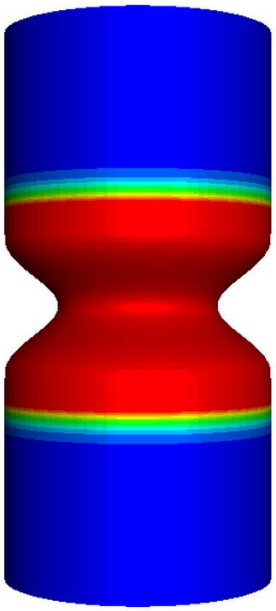

**Figure 11: Illustrative example: von Mises stress contour plot of the deformed shape of the cylinder**

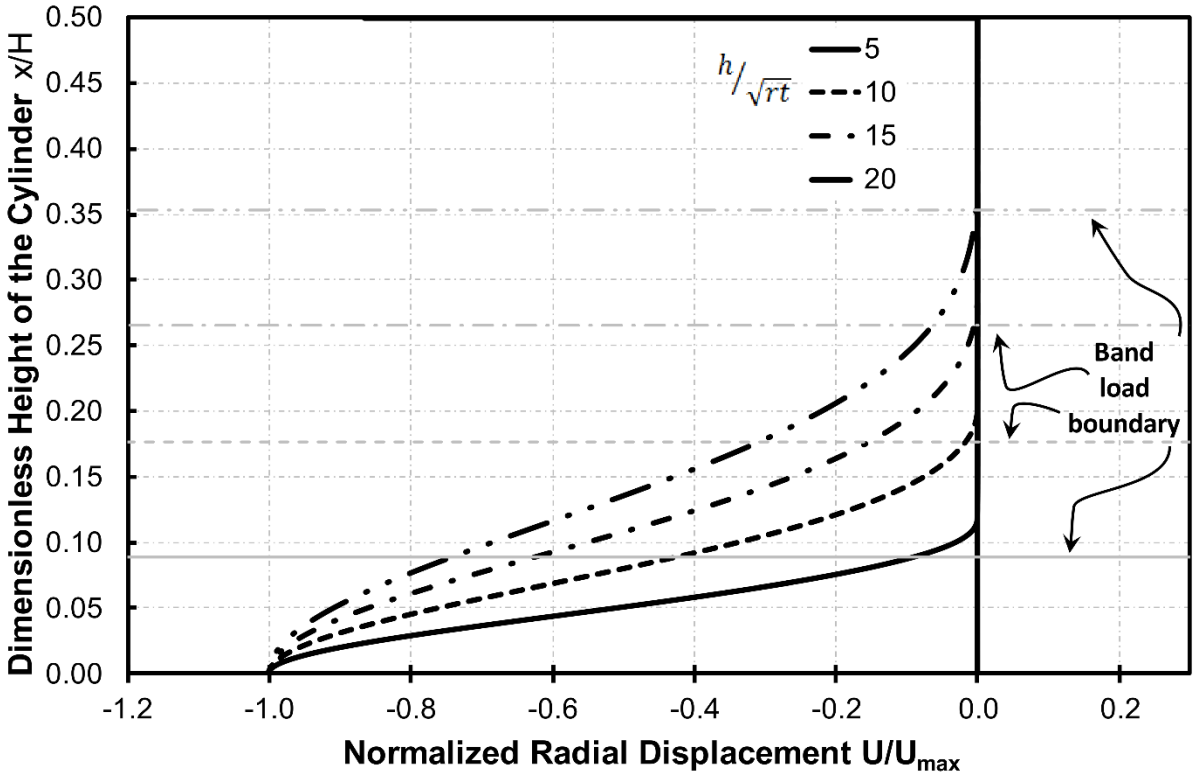


**Figure 12: Dimensionless radial displacement over the height of the cylinder for different band-heights (x=0=mid-height of the cylinder)**

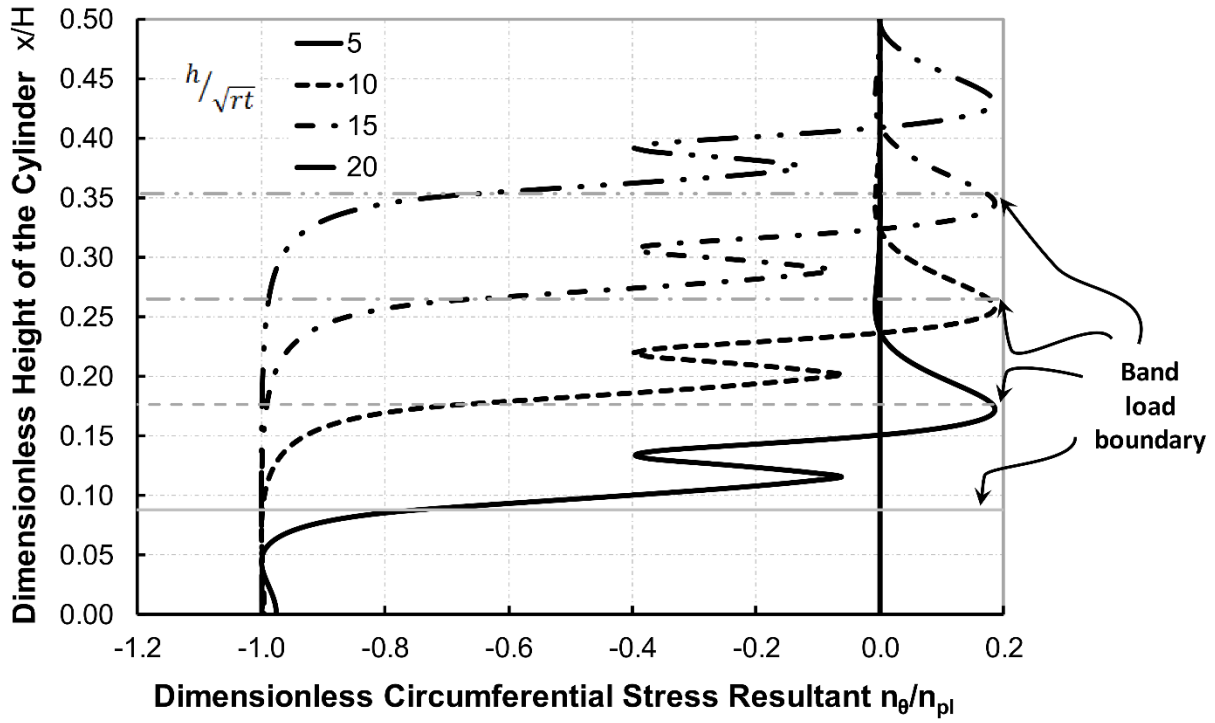


**Figure 13: Dimensionless circumferential stress resultant over the height of the cylinder for different band-heights (x=0=mid-height of the cylinder)**

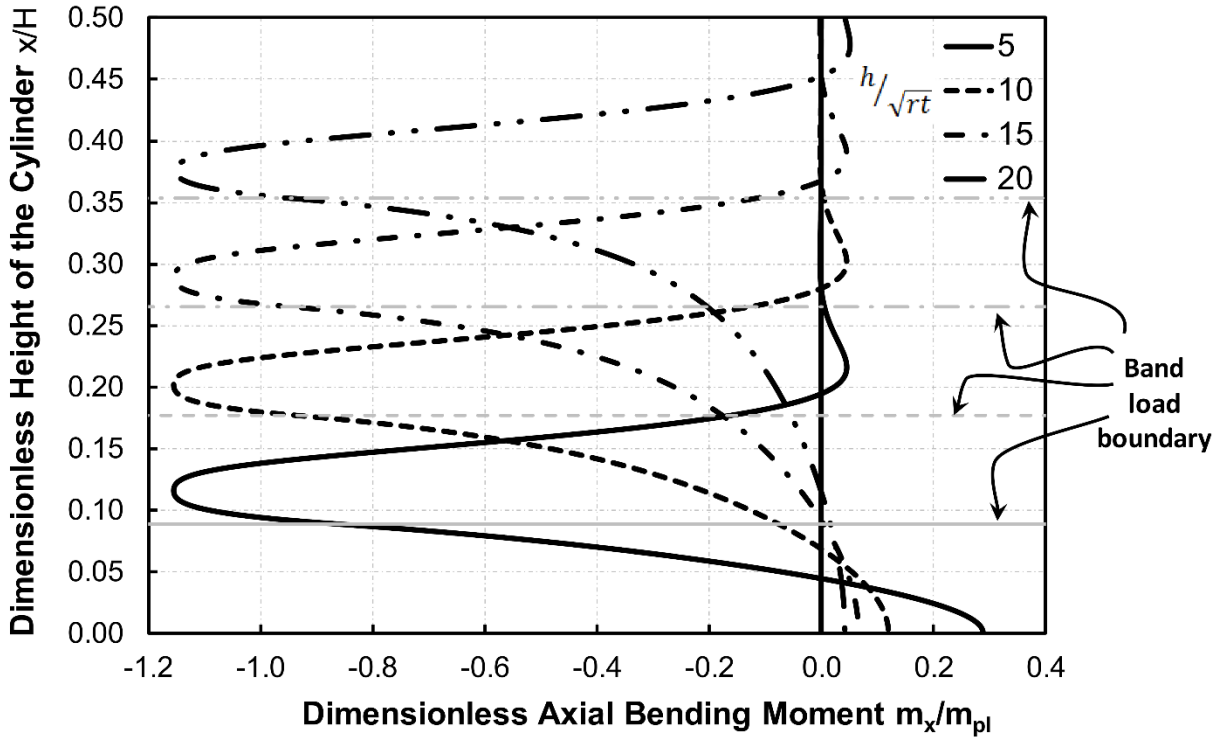


**Figure 14: Dimensionless axial bending moment over the height of the cylinder for different band-heights (x=0=mid-height of the cylinder)**

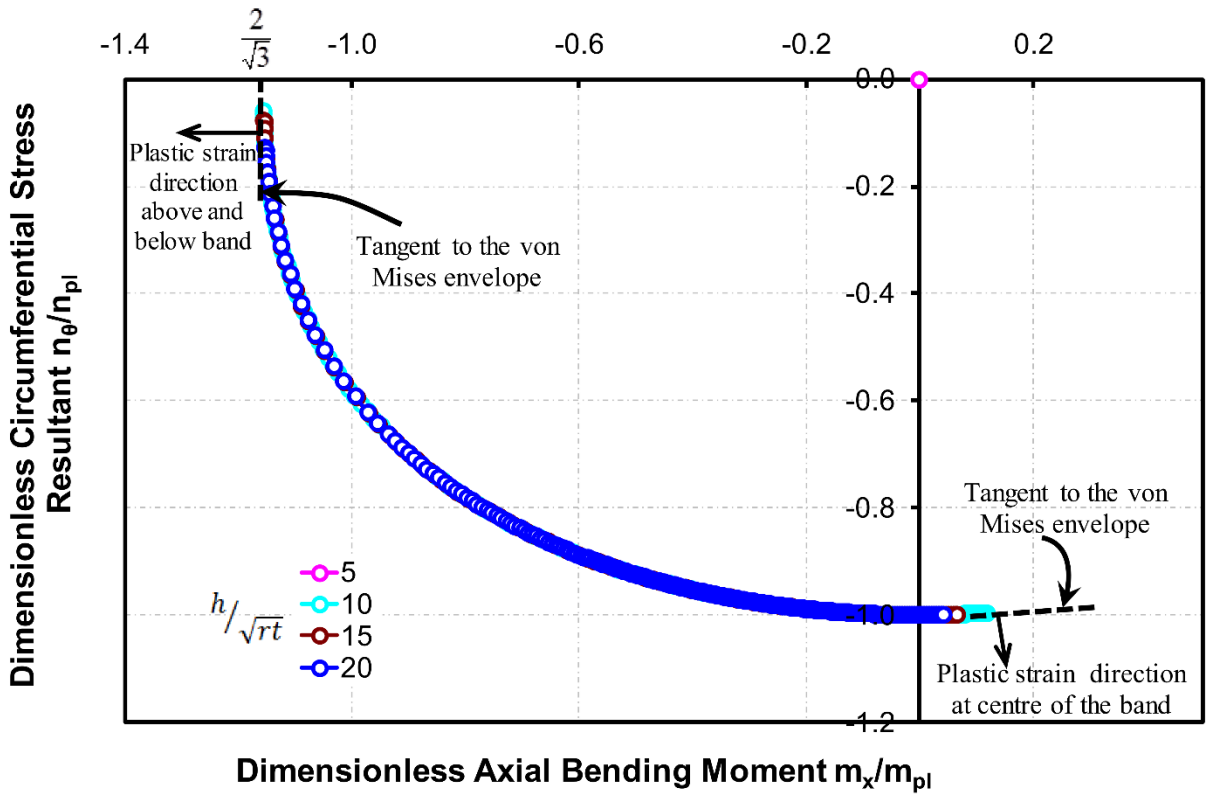


**Figure 15: Plastic membrane - bending interaction stress states in the band**

An analytical solution to this problem was presented by Calladine (1983) using a square yield criterion to approximate the von Mises ellipse (Figure 16). This analysis leads to the dimensionless collapse pressure given by Eqs 7 and 8.

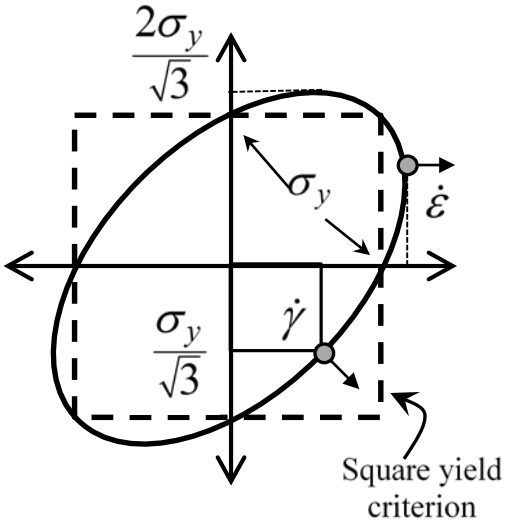


**Figure 16: Von Mises ellipse and square yield criterion**

$$q = \frac{p}{\sigma_y}\frac{r}{t} = \frac{1}{2}\left[1 + \sqrt{\frac{16}{\left(h/\sqrt{rt}\right)^2} + 1}\right] \tag{7}$$

whence

$$\frac{p_{pl}}{\sigma_y} = \frac{t}{2r}\left[1 + \sqrt{\frac{16}{\left(h/\sqrt{rt}\right)^2} + 1}\right] \tag{8}$$

Using the dimensionless collapse pressure $p_{pl}/\sigma_y$ defined by Eqs 7 and 8, a moderately good comparison with the results of full MNA analyses is found (Figure 17) though the analytical treatment systematically overestimates the resistance by about 12%. When the band covers a significant part of the cylinder, the full plastic pressure approaches the value for uniform membrane yield, so the interesting part of this comparison is only for band heights less than around $h/\sqrt{rt}$ =8.

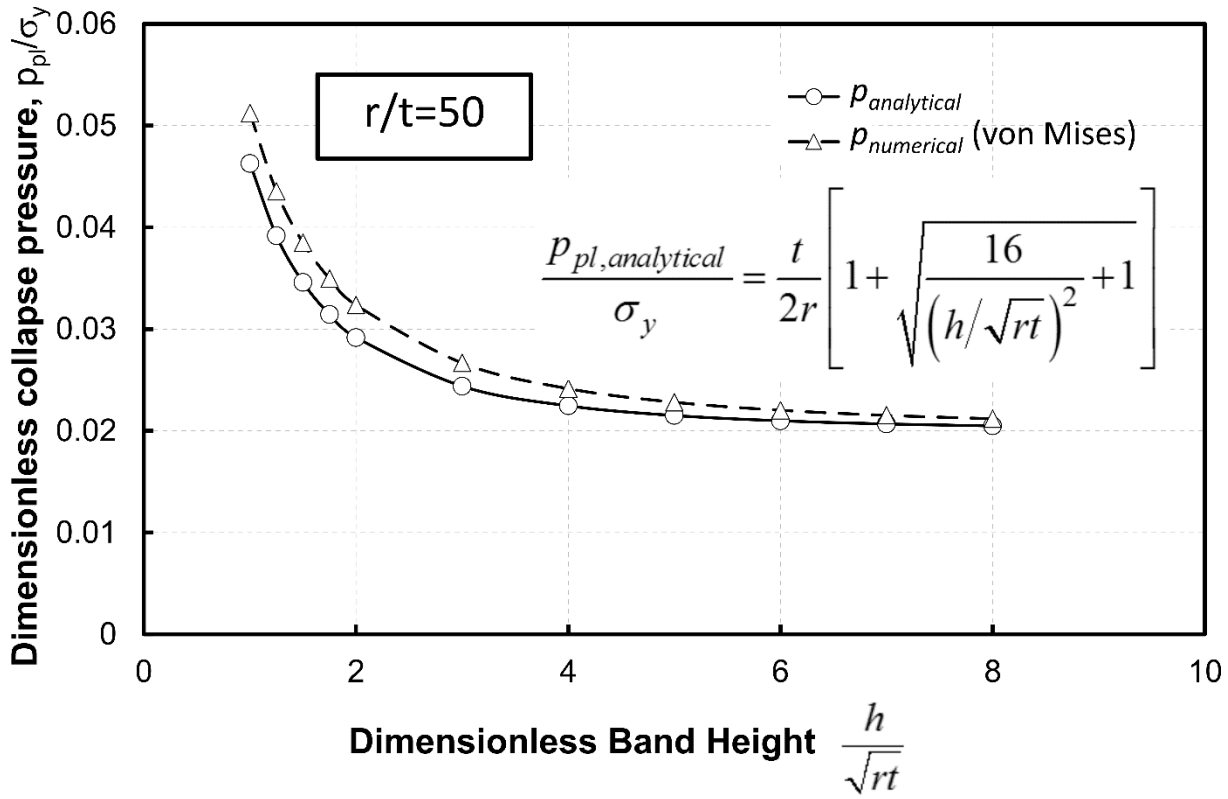


**Figure 17: Comparison of the numerical MNA predictions (von Mises) with the analytical solution (square yield) (Calladine, 1983)**

This analytical solution clearly captures the essential feature of a short band, and is consequently useful when exploring the underlying mechanics of the behaviour. If Calladine's (1983) equation (Eq. 8) is semi-empirically adjusted to produce values associated with the von Mises yield criterion (Eq. 9), a close fit (maximum error 2.9%) to the numerical results is achieved over the full range of $h/\sqrt{rt}$ studied (Figure 18).

$$\frac{p_{pl}}{\sigma_y} = \frac{\sqrt{3}}{2}\cdot\frac{t}{2r}\left[1+\sqrt{\frac{16}{\left(h/\sqrt{rt}\right)^2}+1+\frac{\sqrt{3}}{3}}\right] \tag{9}$$

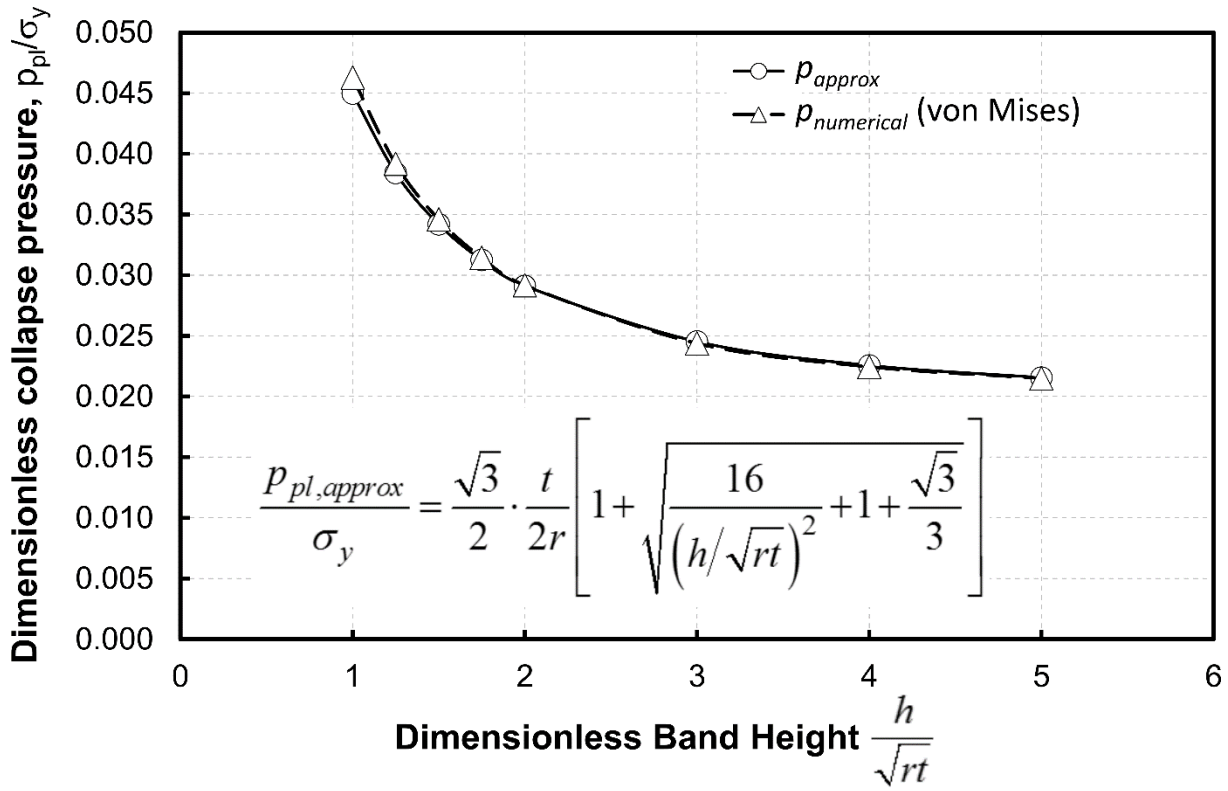


**Figure 18: Empirical adjustment of Calladine's solution to relate to von Mises yield criterion (max error 2.9%)**

The plastic reference load $R_{pl}$ required for use in Reference Resistance Design can now be accurately represented for the geometries investigated in this study using Eq.. 9

A note of caution should be added when calculating a plastic reference load using an MNA analysis. When a plastic limit load analysis (MNA) is performed, geometric nonlinearity is deliberately omitted, and under the strict requirements of EN 1993-1-6 (2007), strain hardening must not be included. The reasons for this choice are explained in Rotter (2005; 2011). The load deflection curve should then display a flat plateau when the plastic collapse load is reached. Ideally, this plateau may then be used to determine the plastic collapse load. However, in many cases involving shells, the software struggles to reach this plateau (Figure 19) because the analysis is non-linear and may involve very high strains where the software may not represent the true behaviour well. At very large displacements (above $U/r$ = 0.02 in Figure 20) the analysis shows some artificial hardening.

The phenomenon of artificial hardening was first described by Holst et al (2005) and more recently

discussed in dos Santos et al (2018). This artificial hardening appears to be only seen with some elements, such as the general purpose element S4R (ABAQUS, 2017), when the analysis considers material nonlinearity without geometric nonlinearity. As soon as geometric nonlinearity is introduced, the artificial hardening disappears, as will be shown in the later sections (Figure 23). In this study, the axisymmetric element SAX1 was used to estimate the plastic collapse load for use in the later sections to achieve computational efficiency. This element does not suffer from the phenomenon of artificial hardening.

However, even when the expected plateau does not develop, the correct plastic collapse load can still be accurately extracted by using the techniques developed by e.g. by Doerich and Rotter (2011a) and dos Santos et al (2018). In this study the work of Holst et al (2005) and Doerich and Rotter (2011a) has been used to extract the plastic collapse load.

The plastic collapse load can be clearly identified by first plotting the data using a modified Southwell plot (Holst et al 2005). The applied load $P$ is plotted against the ratio of the load to a characterising displacement $P/w$ to predict the failure load as a projected intercept on the $P$ axis. Data points that are progressively closer to the true plateau are increasingly closer to the target intercept. In this example, it provides a plastic collapse load 2.7% above the value found using the approximation of Eq. 9 (Figure 20). The second advance in this methodology was an improvement termed the Convergence Indicator Plot (CIP) (Doerich and Rotter, 2011a), which is shown in Figure 21.

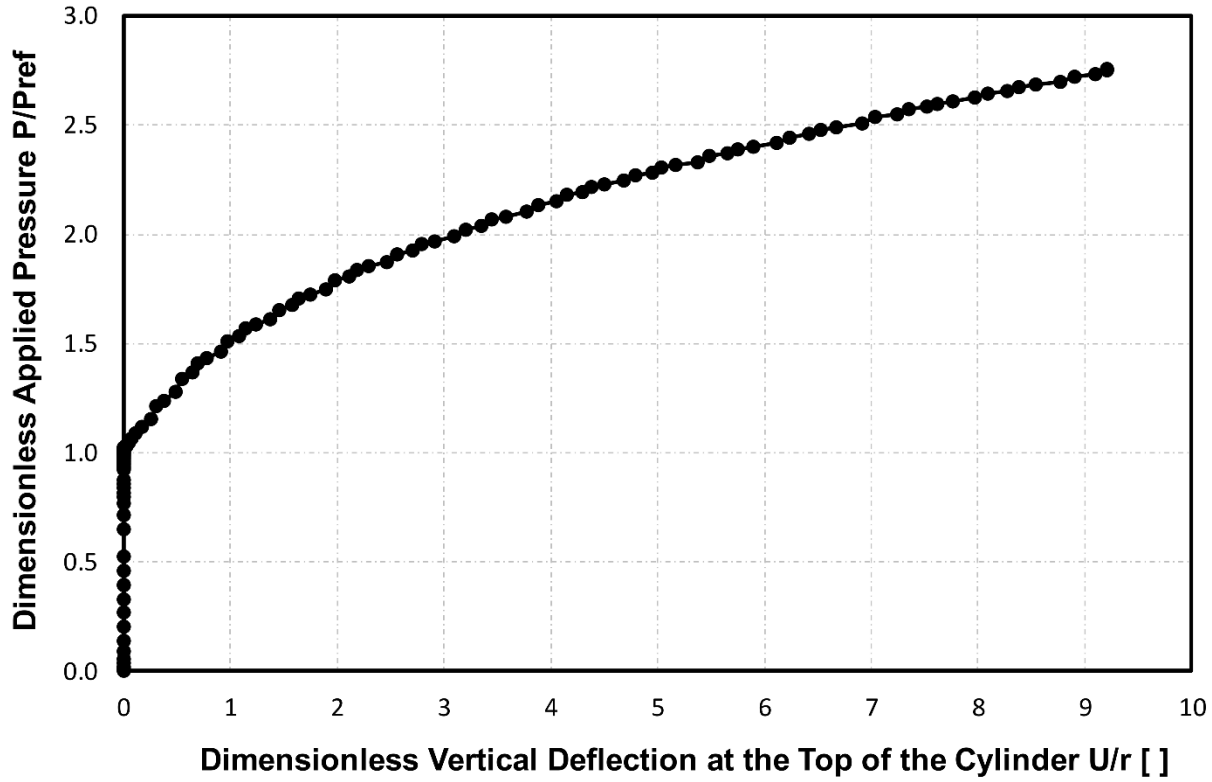


**Figure 19: Example of a load deflection curve using S4R elements**

The CIP plot is based on the on the evaluation of the slope within the modified Southwell plot (Doerich and Rotter, 2011a). Within the elastic plastic region, the modified Southwell plot shows an almost linear behaviour. Using the tangent at any point in the elastic-plastic zone, the intercept of the tangent gives an estimate of the plastic collapse load $P_{MS}$. This estimate may then be compared with the currently applied load level $P_a$ and is expressed as:

$$\omega = \left( P_{MS} - P_a \right) / P_a \tag{10}$$

As ω becomes smaller, the current load level progressively, and close to linear, approaches the plastic collapse load. Repeated precise estimates of the true collapse load are therefore easily obtained, even for problems involving quite complex plastic collapse mechanisms and large plastic strains. However, where spurious hardening occurs, the Southwell plot shows a rapid increase in load at large deflections and this is quickly detected in the CIP plot (Figure 21). Instead, two distinct curves become evident (Figure 21). The original curve is the lower straight line in Figure 21, pointing accurately towards the intercept that is the correct value. As artificial hardening takes

hold, the points abruptly diverge upwards and then follow a different linear line with rising loads and rising deflections. If the initial elastic plastic section of this CIP plot is used, the plastic collapse load is found to be just 0.37% larger than the value given by the approximation of Eq. 9. This illustrates the power of the CIP plot and its capacity to detect errors, as well as giving confidence in the prediction of the correct plastic collapse load even when the software has difficulty in achieving convergence at large deformations.

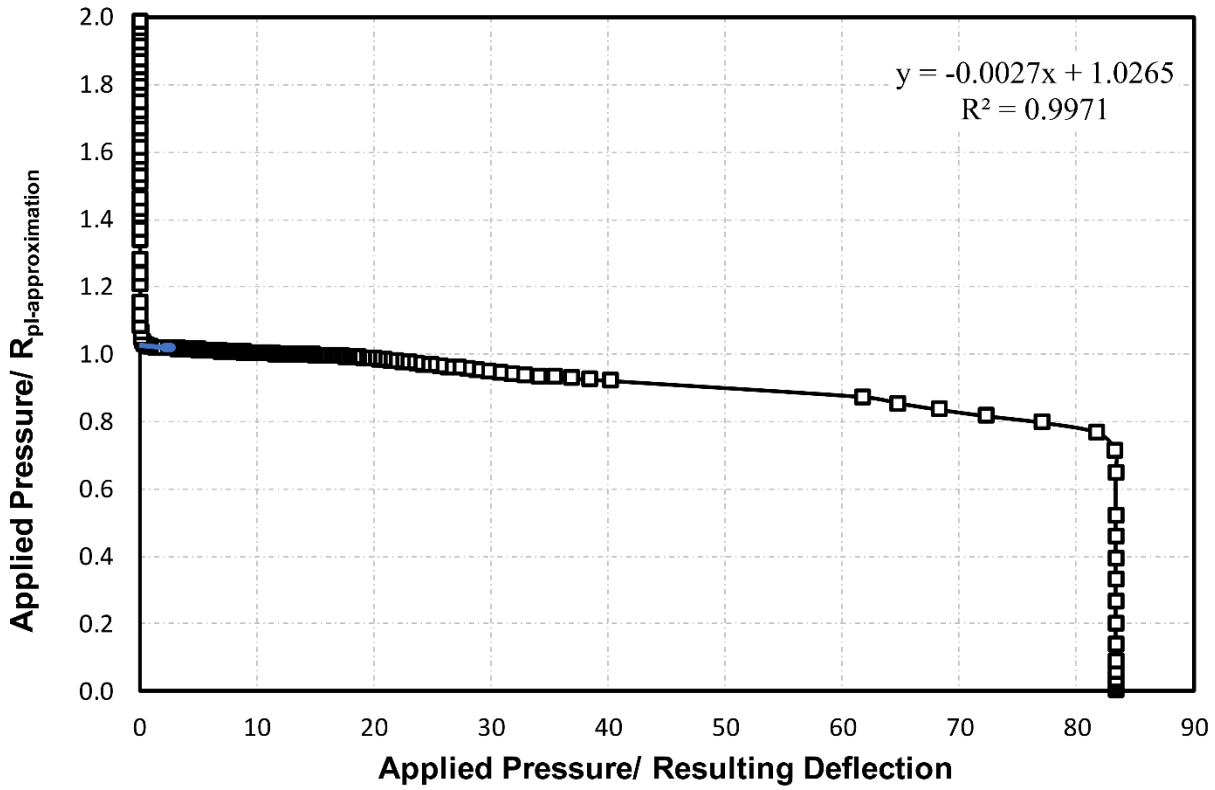


**Figure 20: Determination of the plastic collapse load using the modified Southwell plot (Holst et al., 2005)**

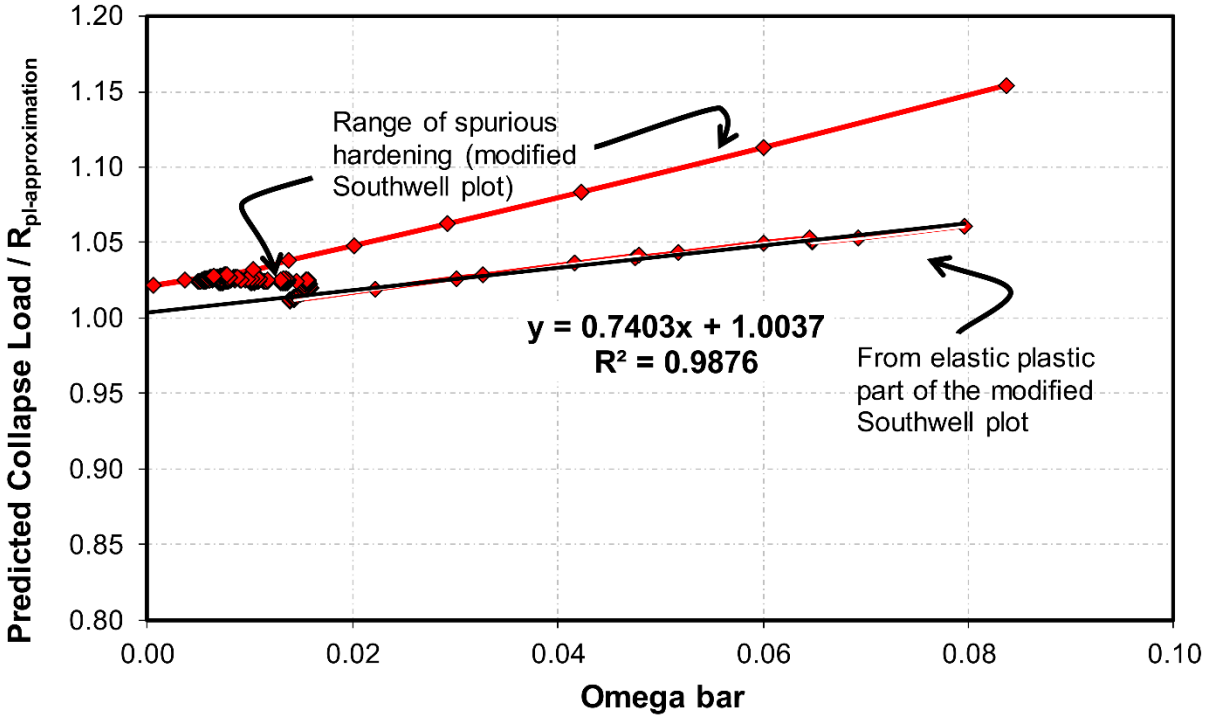


**Figure 21: Convergence Indicator Plot for accurate evaluation of the plastic collapse load**

# 5 Capacity curves

Reference Resistance Design RRD (Rotter, 2016b) allows the designer of thin metal shells to take advantage of the results of complex finite element analysis without the difficulties of setting up and performing these analyses, but instead using hand analysis or spreadsheets and exploiting carefully established research on the relevant problem. The RRD presents the data in the form of a capacity curve, which is already completely defined in terms of the relevant parameters and the reference resistances. To provide a full RRD description, the parameters of the capacity curve for a given loading and boundary conditions must be determined using a geometrically and materially nonlinear analysis of the imperfect structure (GMNIA). Capacity curves (Rotter, 2002; Rotter, 2007; Rotter, 2005) describe the varying resistance of an increasingly slender structure from a fully plastic collapse ($\lambda=\lambda_0$), through plastic buckling, ($\lambda_0<\lambda<\lambda_p$) to elastic buckling in the presence of imperfections ($\lambda>\lambda_p$) (Figure 22) using very few parameters. Each parameter describes a specific physical phenomenon: The plastic range factor $\beta$ identifies the boundary between elastic buckling and elastic plastic failure, the geometric reduction factor $\alpha_G$ describes the influence of geometric nonlinearity in the perfect elastic system and the squash limit relative slenderness $\lambda_0$ defines the upper slenderness limit of fully plastic collapse.

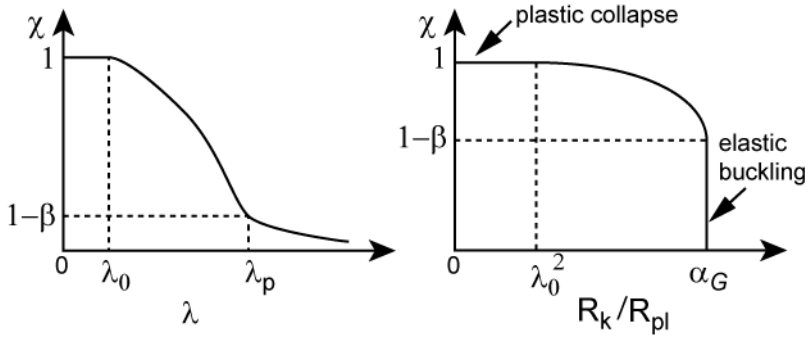


a) b)

**Figure 22: a) General capacity curve b) modified capacity curve (Rotter, 2007; Rotter, 2005)**

The relative slenderness of the system is defined by Eq. (11).

$$\lambda = \sqrt{\frac{R_{pl}}{R_{cr}}} \tag{11}$$

where $R_{pl}$ is the plastic reference resistance derived from an MNA analysis and $R_{cr}$ is the critical buckling resistance derived from an LBA analysis These two resistances have been determined in Sections 3 and 4.

The elastic-plastic buckling reduction factor $\chi$ is defined as

$$\chi = R_k / R_{pl} \tag{12}$$

where the characteristic reference resistance $R_k$ from an experiment or calculated using a GMNIA analysis.

The buckling behaviour of the band loaded cylinder is very similar to that of a uniformly pressurised cylinder with a few long waves around the circumference of the cylinder, even for very short band heights, and the limiting condition of the band load as the uniformly externally pressurised cylinder. Under uniform external pressure, a cylinder is only moderately imperfection sensitive (Greiner, 2004; Guggenberger, 1995; Yamaki, 1984). When the band load acts on only a narrow band, the influence of geometric nonlinearity increases. This effect tends to decrease imperfection sensitivity e.g. (Cai et al., 2002; Doerich, 2007; Sadowski and Rotter, 2011). As a result, the band loaded cylinder is thought to be relatively insensitive to imperfections and this study was consequently limited to the perfect structure and $R_k$ was found using a geometrically and materially nonlinear analysis GMNA.

The capacity curve of EN 1993-1-6 (2007), extended by the adoption of a linearly varying interaction exponent $\eta$ as proposed by Doerich and Rotter (2011b) is given by

$$\chi = 1 \quad \text{when} \quad \lambda \le \lambda_0 \tag{13}$$

$$\chi = 1 - \beta \left( \frac{\lambda - \lambda_0}{\lambda_p - \lambda_0} \right)^{\eta(\lambda)} \quad \text{when} \quad \lambda_0 < \lambda < \lambda_p \tag{14}$$

$$\chi = \alpha / \lambda^2 \quad \text{when} \quad \lambda_p < \lambda \tag{15}$$

with

$$\lambda_p = \sqrt{\alpha / (1 - \beta)} \tag{16}$$

$$\eta(\lambda) = \frac{\eta_0(\lambda_p - \lambda) + \eta_0(\lambda - \lambda_0)}{\lambda_p - \lambda_0} \tag{17}$$

In the case of the perfect shell $\alpha=\alpha_G$ as imperfections are not considered.

The capacity curve describes the effect of varying the dimensionless slenderness of the structure, as described by Rotter (2011), this slenderness can be adjusted easily by using a single geometry and changing the yield stress. This procedure ensures that the effects of geometric nonlinearity stay constant and that reliable values of $\alpha$ can be extracted. It has the added advantage that a single finite element model can be used to generate the full curve. The range of geometries considered here was *r/t*=100, 200, 350, 500, 750, 1000, 2000; *h/r*=0.1, 0.2, 0.3, 0.4, 0.5; and *H/r*=4 with some control samples at *H/r*=10.

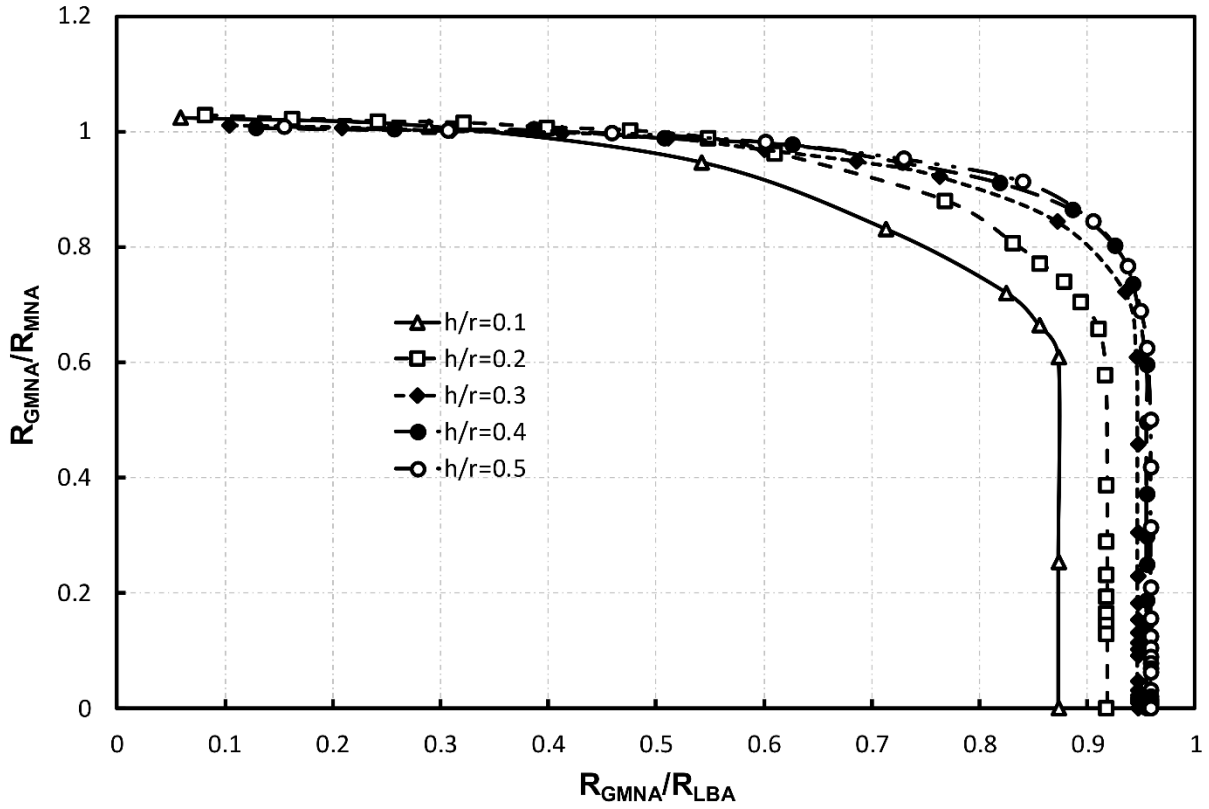


**Figure 23: Modified capacity curves for *r/t*=200 and dimensionless cylinder height H/r=4**

All the calculated capacity curves had a similar form (Figure 23) starting with the plastic range ($\chi\approx1$) for $R_{GMNA}/R_{LBA}$ close to zero and displaying the vertical line of elastic buckling as

$R_{GMNA}/R_{LBA}$ approached unity. The two reference loads ($R_{MNA}$ and $R_{LBA}$) were calculated using the procedures outlined above. It should be noted that the plastic collapse load was calculated using the axisymmetric element SAX1, while all geometrically nonlinear analyses were calculated using the shell element S4R. The characteristic strength $\chi \approx 1$, which shows that the S4R element produces an accurate description of the MNA result under GMNA at very low yield stresses.

The strength reduction due to geometric nonlinearity is small, with the largest reduction at 13% or $\alpha_G$=0.87 (Figure 24). The influence of pre-buckling deformations becomes more pronounced in thicker shells, as is expected from the effect of pre-buckling deformations under uniform external pressure (Yamaki, 1984). The variation in the value of $\alpha_G$ is precisely modelled (within 5%) for a wide range of slendernesses and band heights by Eq. 18 with $C_1$=0.245, $C_2$=8.77×10$^{-5}$ and $C_3$=0.816.

$$\alpha_G = \min\left[C_1\left(\frac{h}{r}\right) + C_2\left(\frac{r}{t}\right) + C_3, 1\right] \tag{18}$$

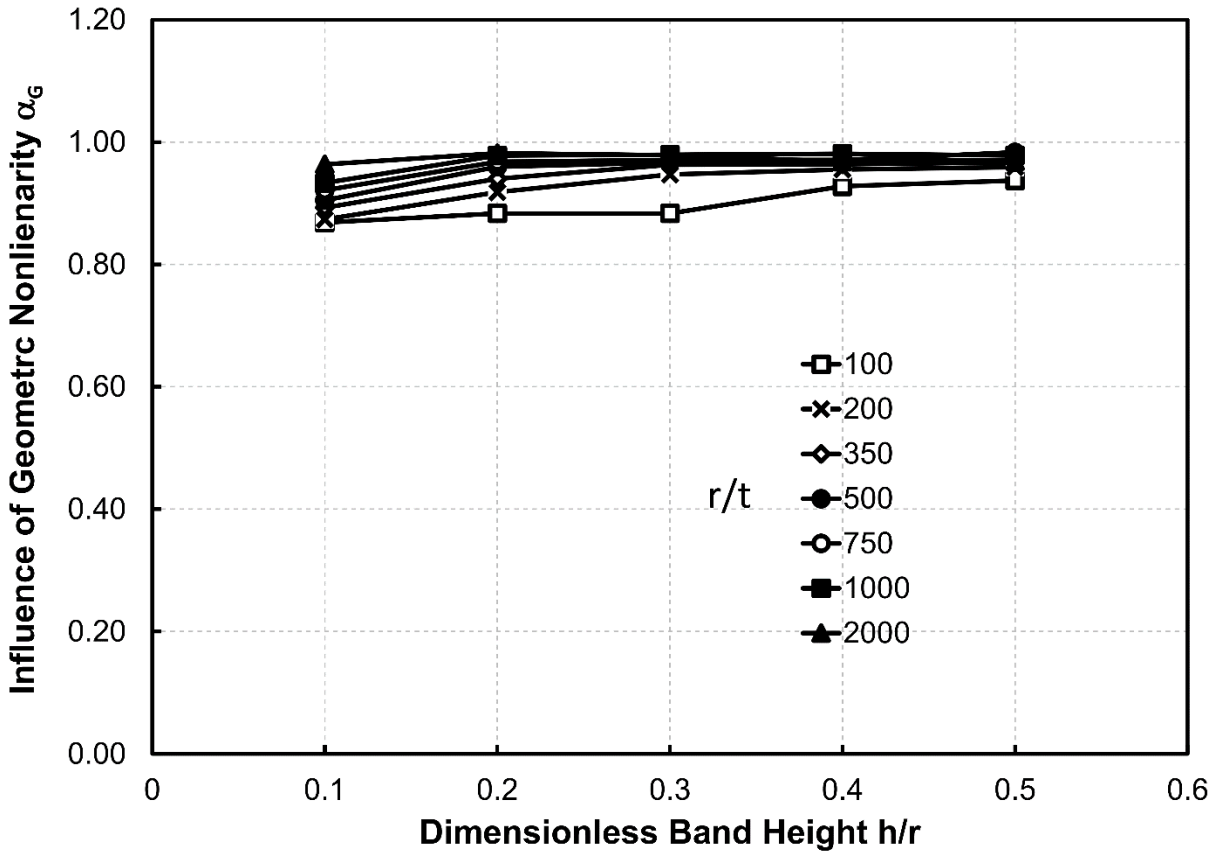


**Figure 24: Influence of geometric nonlinearity**

The boundary between the elastic-plastic range and the elastic buckling range can be found for all geometries at approximately $1-\beta=0.65$ with small variations between 0.63 and 0.67 (i.e. the plastic range factor $\beta= 0.35$ with a variation between 0.33 to 0.37).

For a full design characterisation, the plastic range factor and the squash limit relative slenderness were chosen to be $\beta=0.347$ and $\lambda_0=0$, respectively, for all geometries within the studied range. The interaction coefficients $\eta_0$ and $\eta_p$ were approximated using the limits identified by Doerich and Rotter (2011b) for continuity between domains (Eqs 19 and 20)

$$\eta_p = 2\left(\frac{1-\beta}{\beta}\right)\left(\frac{\lambda_p-\lambda_0}{\lambda_p}\right) \tag{19}$$

$$\eta_0 = 3\left[\frac{1-\beta}{\beta}\right]\left\{1-\frac{\lambda_0}{\lambda_p}\right\}^2 + \frac{1}{2}\eta_p\left(1+\eta_p\right) \tag{20}$$

The resulting set of capacity curves have a maximum error from the original GMNA predictions of about 8% (Figure 25 and Figure 26), slightly under-predicting the dimensionless strength in the elastic plastic domain. The largest discrepancy in the elastic range is 5.7% (Figure 26)

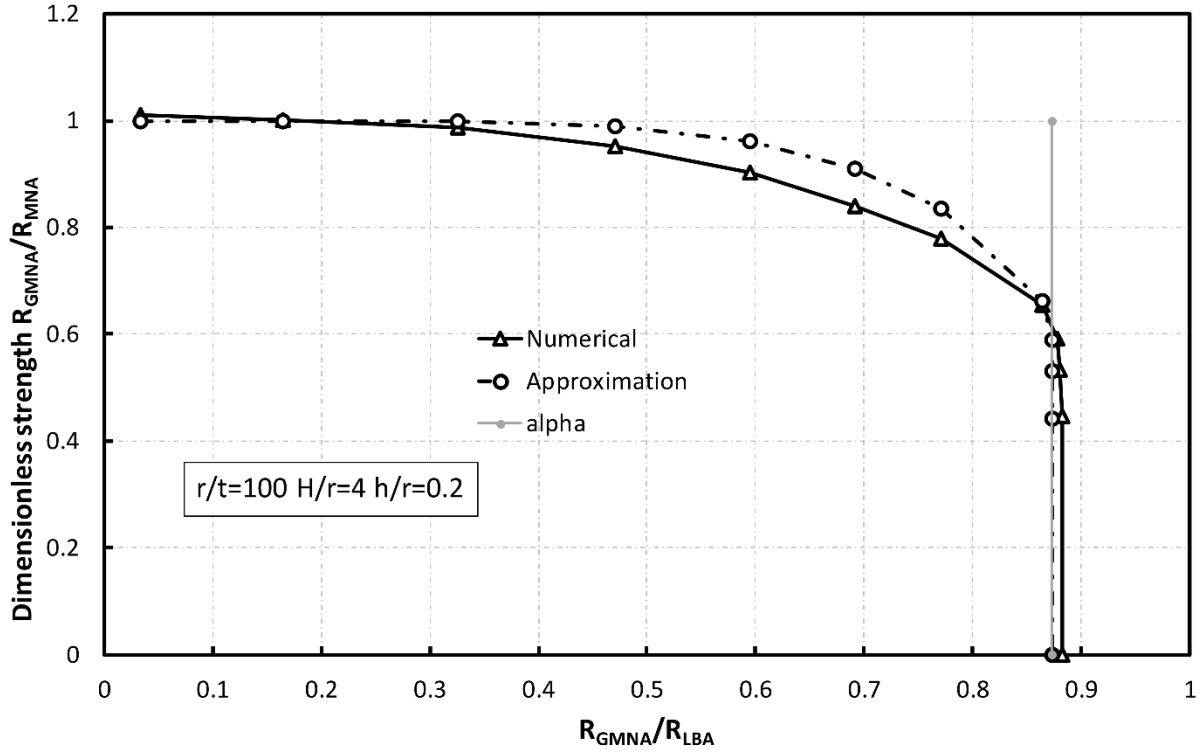


**Figure 25: Example modified capacity curve and its design approximation**

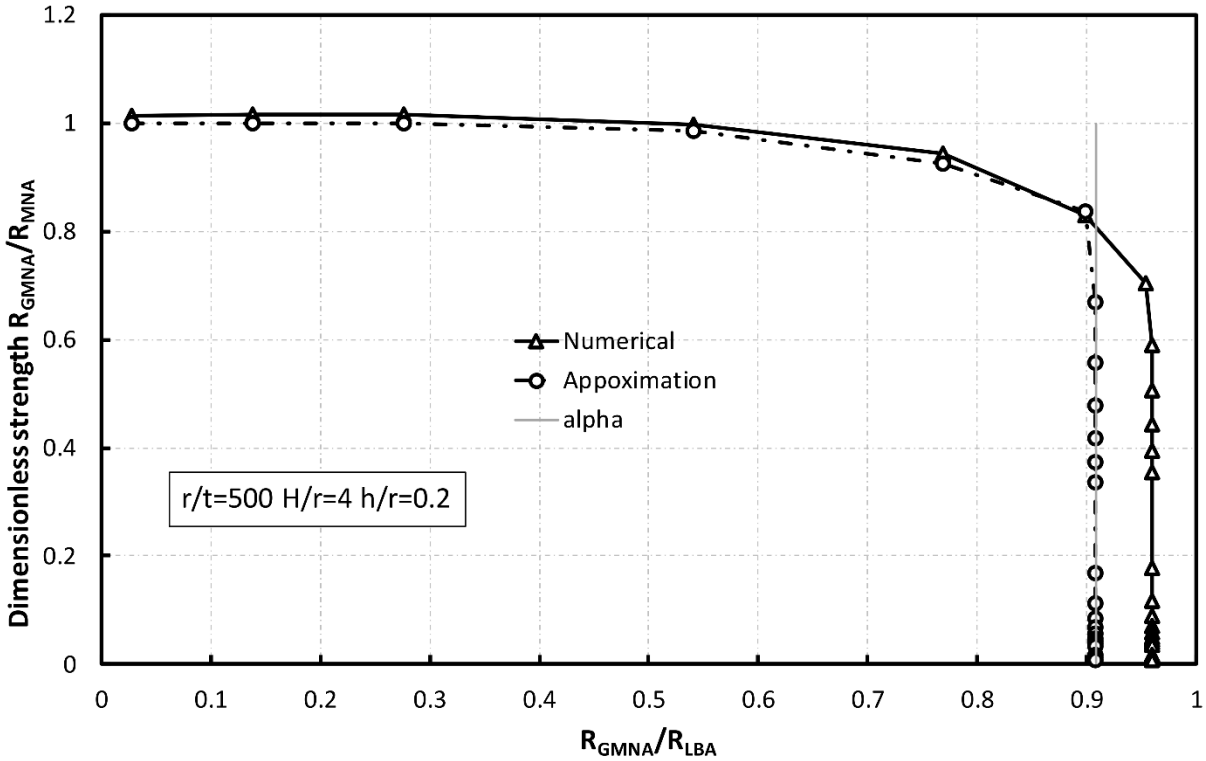


**Figure 26: Example modified capacity curve and its design approximation**

# 6 Conclusion

This paper has presented an investigation into the resistance of thin uniform elastic-plastic cylindrical shells subjected to a band of external pressure at the mid-height. The investigation was conducted within the framework of the Reference Resistance Design (RRD) and accordingly the two required reference loads were investigated first: the critical buckling resistance ratio $R_{cr}$ derived from an LBA analysis and the plastic reference resistance ratio $R_{pl}$ derived from an MNA analysis.

It has provided precise approximate formulae for the elastic critical buckling pressure $p_{cr}$ and the plastic collapse pressure $p_{pl}$. Both approximations compare well with the numerical data within the range of geometries investigated $H/r>4$, $h/r<0.5$ $100< r/t<2000$.

The linear bifurcation analysis mostly showed long vertical buckles over the full height of the cylinder but with the number of circumferential modal waves that reduced as the band width rose. These modes were similar to those for cylinders under uniform external pressure. The buckling pressures were expected to depend strongly on the full height of the cylinder, but they were found instead to depend only on the band height for most practical geometries. The critical buckling pressure was found to be dominated by the total applied external load, even when the same buckling mode is invoked at different band widths.

The results of the materially nonlinear analysis using the von Mises yield criterion compare well with the analysis of Calladine (1983) though the latter was found to be slightly unconservative. A minor semi-empirical adjustment of Calladine's result produced an excellent approximation to the numerical results.

The collapse mechanism couples stretching and bending plastic deformations in different proportions at different points in the shell with the maximum deflection at the mid-height of the cylinder. The plastic strain field near the load is dominated by yielding due to stretching. The study of the plastic strain vectors and location of different points in the cylinder on the yield surface illustrated well the complex behaviour of mechanisms in shell structures.

Capacity curves for the full range of geometries ($H/r>4$, $h/r<0.5$, $100<r/t<2000$) were generated

and interpreted within the Reference Resistance Design (RRD). A summary of the extracted parameters for use in design can be found in Table 1.

It was found that geometric nonlinearity influences the behaviour only slightly in the elastic range, with the greatest impact being $\alpha_G$=0.87 for the thickest ($r/t$=100) cylinder investigated.

| | |
|---|---|
| $\beta$ | 0.347 |
| $\lambda_0$ | 0 |
| $\alpha_G = \min\left[ C_1\left(\frac{h}{r}\right) + C_2\left(\frac{r}{t}\right) + C_3, 1 \right]$ | |
| $\eta_p = 2\left(\frac{1-\beta}{\beta}\right)\left(\frac{\lambda_p - \lambda_0}{\lambda_p}\right)$ | |
| $\eta_0 = 3\left[\frac{1-\beta}{\beta}\right]\left\{1-\frac{\lambda_0}{\lambda_p}\right\}^2 + \frac{1}{2}\eta_p\left(1+\eta_p\right)$ | |

**Table 1: Summary of the parameters for Reference Resistance Design**

The strength of a band loaded perfect cylinder, within the defined range of geometries, can now be calculated by hand using the characterisation of Reference Resistance Design.

It has been shown that even when the plastic collapse analysis does not develop a clear plateau the plastic collapse load can be accurately extracted using the techniques of the modified Southwell plot and CIP plot, both devised by Doerich and Rotter (2011a) .

# References

ABAQUS (2017) *Commercial FE Software and Documentation.* Providence, RI, USA.: Dassault Systèmes, Simulia Corporation.

Batdorf S (1947) *A Simplified Method of Elastic-Stability Analysis for Thin Cylindrical Shells.* Langley Field, Va.: National Advisory committee for aeronautics.

Brush DO and Almroth BO (1975) *Buckling of Bars, Plates, and Shells.* US: McGraw-Hill Inc.

Cai M, Holst J and Rotter JM (2002) *Buckling Strength of Thin Cylindrical Shells Under Localized Axial Compression.*

Calladine CR (1983) *Theory of Shell Structures.* Cambridge: Cambridge University Press.

Doerich C (2007) Strength and Stability of Locally Supported Cylinders. Phd, University of Edinburgh.

Doerich C and Rotter JM (2011a) Accurate determination of plastic collapse loads from finite element analyses. *Journal of Pressure Vessel Technology, Transactions of the ASME* 133(1).

Doerich C and Rotter JM (2011b) Generalised capacity curves for stability and plasticity: Application and limitations. *Thin-Walled Structures* 49(9): 1132-1140.

dos Santos G, Gardner L and Kucukler M (2018) A method for the numerical derivation of plastic collapse loads. *Thin-Walled Structures* 124: 258-277.

Ebner H (1952) Theoretical and experimental investigations on buckling of cylindrical tanks subjected to external pressure. *Stahlbau* 21: 153-159.

EN1993-1-6 (2007) *Eurocode 3: Design of Steel Structures. Part 1-6: Strength and Stability of Shell Structures.* Brussels: CEN, European Committee for Standardization.

Greiner R (2004) Cylindrical shells under uniform external pressure. In: Teng J and Rotter JM (eds) *Buckling of Thin Metal Shells.* London: Spon Press, 154-174.

Guggenberger W (1995) *Buckling and Postbuckling of Imperfect Cylindrical Shells Under External Pressure.*

Holst JMFG, Doerich C and Rotter JM (2005) *Accurate Determination of the Plastic Collapse Loads of Shells when using Finite Element Analyses.* Amsterdam: Elsevier Ltd.

Rotter JM (2016a) *Advances in Understanding Shell Buckling Phenomena and their Characterisation for Practical Design.* Zielona Góra, Poland: CRC Press.

Rotter JM (2016b) *The New Method of Reference Resistance Design for Shell Structures.* Timisoara, Romania: Wiley.

Rotter JM and Schmidt H (2014) *Buckling of Steel Shells: European Design Recommendations.* ECCS: European Convention for Constructional Steelwork.

Rotter JM (2002) Shell buckling and collapse analysis for structural design. In: Drew HR and Pellegrino S (eds) *New Approaches to Structural Mechanics, Shells and Biological Structures.* Netherlands: Springer, 355-378.

Rotter JM (2007) *Recent Advances in the Philosophy of the Practical Design of Shell Structures, Implemented in Eurocode Provisions.* Rotterdam, The Netherlands: Millpress.

Rotter JM (2011) Shell buckling design and assessment and the LBA-MNA methodology. *Stahlbau* 80(11): 791-803.

Rotter JM (2005) Stability and plasticity in structural analysis: A new conceptual framework. In: Shen ZY, , Li GQ and Chan SL (eds) *Fourth International Conference on Advances in Steel Structures.* Oxford: Elsevier Science Ltd, 1815-1826.

Sadowski AJ and Rotter J (2011) Steel silos with different aspect ratios: II—behaviour under eccentric discharge. *Journal of Constructional Steel Research* 67(10): 1545-1553.

Sadowski AJ, Fajuyitan OK and Wang J (2017) A computational strategy to establish algebraic parameters for the Reference Resistance Design of metal shell structures. *Advances in Engineering Software* 109: 15-30.

Save MA and Massonnet CE (1972) *Plastic Analysis and Design of Plates, Shells and Disks.* : North-Holland.

Teng J (2004) Shell junctions. In: Teng J and Rotter JM (eds) *Buckling of Thin Metal Shells.* London: Spon Press, 369-408.

Teng J and Rotter J (1992) Recent research on the behaviour and design of steel silo hoppers and transition junctions. *Journal of Constructional Steel Research* 23(1-3): 313-343.

Teng J and Rotter J (1991a) Plastic buckling of rings at steel silo transition junctions. *Journal of Constructional Steel Research* 19(1): 1-18.

Teng J and Rotter JM (1991b) Collapse Behavior and Strength of Steel Silo Transition Junctions. Part I: Collapse Mechanics. *Journal of Structural Engineering* 117(12): 3587-3604.

Teng J and Rotter JM (1991c) Collapse Behavior and Strength of Steel Silo Transition Junctions. Part II: Parametric Study. *Journal of Structural Engineering* 117(12): 3605-3622.

Yamaki N (1984) *Elastic Stability of Circular Cylindrical Shells.* Amsterdam: Elsevier.